Revisiting the atmospheric dynamics of the two century floods over north-eastern Italy

Francesco Sioni[a,*], Silvio Davolio[b], Federico Grazzini[c,d], Lorenzo Giovannini[e]

[a] *Osservatorio Meteorologico Regionale OSMER-ARPA FVG, Palmanova, Italy*
[b] *Institute of Atmospheric Sciences and Climate, National Research Council of Italy, CNR-ISAC, Bologna, Italy*
[c] *Ludwig-Maximilians-Universitat, Meteorologisches Institut, Munich, Germany*
[d] *ARPAE-SIMC, Regione Emilia-Romagna, Bologna, Italy*
[e] *Department of Civil, Environmental and Mechanical Engineering, University of Trento, Trento, Italy*

Abstract

The two most intense precipitation events that occurred over northern and central Italy in the last century are analyzed in this study: the November 1966 flood and the Vaia storm in October 2018. These two events share a similar large-scale evolution, characterized by a vigorous baroclinic wave, deepening on the western Mediterranean basin and slowly evolving eastward. Although this is a common synoptic setting for severe weather over Italy in autumn, in these cases the interaction between incoming Rossby wave packets produced a particularly strong downstream development over the Mediterranean. In both events, the large-scale dynamics was able to focus towards the Mediterranean basin an exceptional high amount of moisture transported from the Tropics in the form of Atmospheric Rivers (ARs), although with local and remote differences related with the sea and atmospheric state conditions characterizing these two episodes occurring 52 years apart. As a result, the precipitation patterns, in terms of both duration, intensity and distribution, were quite different: while in 1966 heavy rainfall affected for 48 hours mostly Tuscany region (infamous Florence flood) and north-eastern Italy, in 2018 almost the entire Alpine chain, as well as Liguria region and central Italy, were hit by severe events during almost three days. Only over the north-eastern Italian Alps the rainfall fields look similar in the two events.

*Corresponding author.
Email address: francesco.sioni@meteo.fvg.it (Francesco Sioni)

The mesoscale dynamics and the moisture supplies are investigated in detail, highlighting peculiarities and common aspects. It is found that the different characteristics of the ARs (intensity and steadiness) partially explain the rainfall patterns, but the complete picture has to take into account also local (e.g. Mediterranean) sources of moisture and smaller scale circulation features that turned out to be relevant. Through a relative comparison, this study points out some important aspects of the genesis of extreme precipitation events over Italy, identifying important precursors and moisture sources. In an operational context, this may help to recognize the environmental conditions potentially leading to the most severe precipitation episodes.

Keywords: extreme precipitation events, EPE, Vaia, 66 flood, BOLAM, atmospheric rivers, AR, RWP

---

1. Introduction

In the Mediterranean basin, many areas are frequently threatened by heavy precipitation events and floods, responsible for damages and casualties. The Italian peninsula, extending in the central Mediterranean Sea and characterized by complex terrain, is particularly prone and exposed to natural hazards caused by intense precipitations.

The main purpose of this study is to characterize the two most intense precipitation events over northern and central Italy in the last 60 years: the 1966 flood occurred between 3 - 5 November 1966 (commonly known in Italy as 'century' flood) and the Vaia storm between 27 - 30 October 2018. Vaia is the name given by the Free University of Berlin to the cyclone developed over the Tyrrhenian Sea on 28 October and it is commonly used to refer to all the high-impact weather phenomena associated to the event. These two extreme precipitation events (EPEs) have affected the largest area over northern and central Italy with the highest amount of precipitation volume since 1961 (Grazzini et al., 2020). Understanding the physical mechanisms at the basis of these exceptional meteorological events is of fundamental importance for the prevention of impacts, especially in relation to future climate change scenarios (Myhre et al., 2019).

During the 1966 flood, the persistently high precipitation rate led to the breaking of the river banks of Arno and Ombrone in Tuscany, responsible for the infamous flood of Florence (De Zolt et al., 2006). Also over northern Italy, the Adige river in Trento and the Tagliamento river in the Friuli-Venezia

Giulia (FVG) plain caused extensive floods. The North Adriatic coast was struck by storm surges and high sea waves. Venice was deeply affected with the maximum sea level ever recorded (194 cm) since the beginning of sea level records in 1872. The most affected areas were the eastern Alps and Pre-Alps, where rainfall attained 751 mm in 48 hours in Barcis (FVG region) (Malguzzi et al., 2006).

The impacts of the Vaia event were associate not only with heavy rain, flooding episodes and storm surges, but also with landslides and especially extreme wind storms (Cavaleri et al., 2019). The highest precipitation amounts recorded in 5 days were 817 mm at Malga Chiampiuz (FVG region), of which 385 mm in only one day (28 October), 716 mm at Soffranco (Veneto region) and 623 mm at Torriglia (Liguria region). The fierce wind, that severely damaged more than 41,000 ha of forests (Motta et al., 2018), attained extreme values over the Alps with maximum recorded gust values exceeding 50 m s^{-1} (Giovannini et al., 2021) at some locations. The more severe damages due to precipitation in 1966 with respect to Vaia were probably related to the situation in the period preceding the EPEs. In 1966, frequent precipitation episodes developed in the months before the event reducing the storage capacity of the soils. On the other hand, Vaia came after a dry period and river discharges were low at the time of the event.

EPEs over northern and central Italy are generally driven by large scale dynamics and are associated with upper-level synoptic waves or Rossby waves (Lorenz, 1972; Hoskins and Ambrizzi, 1993), organized in Rossby wave packets (RWPs) (Wirth et al., 2018). In addition to the dynamical forcing, a key element for EPEs occurrence is moisture availability. Moisture can be provided by local sources (e.g. evaporation from the Mediterranean Sea, Duffourg and Ducrocq, 2013) or by transport from remote regions, which often occurs ahead of an extratropical cyclone or a trough extending over the western Mediterranean. In the present study, water vapour (WV) transport is investigated especially in relation to Atmospheric Rivers (ARs) (Ralph et al., 2020). ARs are defined as long and relatively narrow filaments of intense horizontal WV transport that are located ahead of a cold front of an extratropical cyclone (AMS, 2022) and that are able to trigger heavy or extreme precipitation events where they are forced to lift over an orographic barrier (Gimeno et al., 2014). The presence of an AR was revealed by Davolio et al., 2020a in the Vaia event and suggested by several authors (Krichak et al., 2015; Berto et al., 2005; Malguzzi et al. 2006) for the 1966 flood, using respectively a specific detection algorithm or analyzing the integrated vapour

transport (IVT) field.

EPEs over northern Italy have been investigated by Grazzini et al. (Grazzini et al., 2020 ; Grazzini et al., 2021) and systematically subdivided in 3 categories (Cat1, Cat2, Cat3) using machine-learning unsupervised K-means clustering. Cat1 events develop from November to April and are associated mainly with statically stable moist marine air at low levels that is lifted by orographic barriers. Cat3 events are frequent in summer months and are associated with local non-equilibrium convection (Done et al., 2006) triggered by thermal boundaries and shaped as single cells or mesoscale convective systems (MCS). Cat2 events show intermediate features between Cat1 and Cat3: they occur mainly during autumn and are triggered by frontal uplift with embedded deep convection. Both 1966 flood and Vaia storm belong to Cat2 events, that include most of the EPEs leading to the most severe floods over northern Italy (Grazzini et al., 2020).

This work adopts different tools and methods in order to compare the events in terms of both synoptic evolution and WV transport, which are two critical aspects in the formation of EPEs (De Vries, 2021). A fundamental dynamical process leading to EPEs development is Rossby wave breaking (RWB) due to dynamic instabilities. RWB, which is often associated with stratospheric wave intrusion, may induce cyclogenesis at the surface (Raveh-Rubin and Flaounas, 2017) and steer intense moisture transport towards the region of extreme precipitation. Intense WV flows, combined with the strong dynamic activity in the downstream region of the trough, create the ideal conditions for the development of EPEs. Ascent and deep moist convection are also favoured by the reduced static stability and by the interaction with the orography.

In light of the discussed theoretical background, the atmospheric dynamics of the two EPEs is first analyzed using recently available datasets (ERA5, ArCIS) and then simulated using the numerical meteorological model BOLAM. This study extends the results of Davolio et al., 2020a, exploiting the same diagnostic tools (atmospheric water budget computation) to highlight similarities and differences between the two EPEs. The analysis focuses on the description of both large-scale and mesoscale phenomena, especially concerning WV transport and its origins, and aims at explaining the different observed precipitation patterns in the two events in terms of the characteristics of this transport.

The paper is organized as follows. Section 2 presents the datasets and the tools used for the analysis of the two EPEs, whose synoptic characteristics are

described in Section 3. The analysis of model results is presented in Section 4, focusing in particular on the WV budget technique, while conclusions are drawn in Section 5.

2. Datasets and methods

2.1. Datasets

Reanalysis data are retrieved from the European Centre for Medium-Range Weather Forecasts (ECMWF) ERA5 database (Hersbach et al., 2020), using the preliminary version of the ERA5 back-extension (1950-1978) to study the 1966 flood. In this way it is possible to study the two EPEs that occurred more than 50 years apart with the same dataset, available at hourly interval at a spatial resolution of 0.25°.

Precipitation data for central and northern Italy are retrieved from the ArCIS (Archivio-Climatologico per l'Italia Centro-Settentrionale) database (Pavan et al., 2019). ArCIS is a gridded precipitation dataset, with a resolution of approximately 5 km, derived from 1,762 rain-gauges that belong to different networks of 11 Italian regions, plus several stations of adjacent Alpine areas, recently assembled by the regional services. ArCIS provides daily cumulated precipitation over central and northern Italy for the period 1961 to present. Input data undergo a quality check concerning time consistency, synchronicity, and statistical homogeneity. Spatial interpolation is applied on original data using a modified Shepard scheme (Antolini et al., 2016).

2.2. The numerical weather prediction model: BOLAM

BOLAM (BOlogna Limited Area Model) is a hydrostatic limited-area model developed at the Institute of Atmospheric Sciences and Climate of the Italian National Research Council (CNR-ISAC) in Bologna since the early 90's (Buzzi et al., 1994). The model integrates the primitive equations on a rotated lat-lon grid. Prognostic variables are defined on a staggered Arakawa C grid, while the vertical discretization is based on a regular Lorenz grid. BOLAM uses a hybrid vertical coordinate system, in which the terrain-following coordinate σ relaxes to a pressure coordinate with increasing height above the ground. The temporal integration scheme is split-explicit and forward-backward for the gravity modes.

Atmospheric radiation is computed based on a combined application of the Ritter and Geleyn (Ritter and Geleyn, 1992) and the ECMWF schemes

(Morcrette et al., 2008). The turbulence scheme is based on a 1.5-order closure parameterization, with a prognostic equation for the turbulent kinetic energy (including advection) (Zampieri et al., 2005). Deep convection is based on a modified version of the Kain-Fritsch scheme (Kain, 2004), and the microphysical processes are treated with a simplified approach, suitable for non-convection-resolving models (Buzzi et al., 2014). The 7-layer soil model computes surface energy, momentum, water and snow balances, heat and water vertical transfer, vegetation effects at the surface and in the soil. It takes into account the observed geographical distribution of different soil types, vegetation coverage and soil physical parameters. A simple slab ocean model evolves the sea surface temperature depending on radiative and latent/sensible heat surface fluxes. For further details on BOLAM refer to Buzzi et al., 2014 and Davolio et al., 2020b.

In the present study initial and boundary conditions are provided by 3-hourly ERA5 analysis fields and imposed through a relaxation scheme. The integration domain of the simulations is shown in Fig. 1 and has a spatial resolution of 0.1°, corresponding to approximately 11 km. For the 1966 flood the simulation is initialized on 3 November 1966 at 00 UTC and ends on 5 November 1966 at 12 UTC (60 hours). The simulation for the Vaia storm is initialized on 26 October 2018 at 12 UTC and ends on 30 October at 00 UTC (84 hours). It is worth noting that different simulations were performed for the 1966 event, with an earlier initialization time, to study the AR in its early stage, well before its arrival over the Mediterranean basin. However, all the simulations initialized on 2 November, respectively at 00, 06, 12 and 18 UTC were not able to capture the correct localization of the EPE, due to a wrong synoptic evolution. These results highlight a quite large uncertainty in the prediction of this event, as also pointed out in Capecchi and Buizza, 2019.

2.3. Water budget diagnostic

A water budget diagnostic technique has been applied to the BOLAM output to characterize the origin and amount of moisture feeding the precipitation systems and to evaluate the local contribution of evaporation from the Mediterranean Sea with respect to remote moisture sources.

An atmospheric box is considered with the upper face at a specific pressure level and the lower face at the surface. The idea is to calculate the eulerian variation in time of atmospheric water (all the different water species

are considered, namely vapour, water, and ice) inside the box. In particular, the processes that contribute to a substantial variation of water (ΔIW) inside the box are the horizontal transport (F) through the lateral faces, evaporation (E) from the sea surface and precipitation (P). The equation that regulates these fluxes is:

$$\Delta IW = E + FS + FN + FE + FW - P + Res \tag{1}$$

where FS, FN, FE and FW indicate the fluxes across each lateral face of the box (South, North, East and West), while *Res* accounts for numerical residuals, due to interpolation and time-space discretization. Positive fluxes are associated with inflow into the box, negative fluxes with outflow. The terms are expressed in kg s^{-1}, and their detailed computation is described in Davolio et al., 2020a. The budget terms are calculated every 15 minutes, in order to minimize errors due to time discretization. The water fluxes are instantaneous values; precipitation and evaporation, instead, are integrated values and they have to be converted to instantaneous rates as well.

First, the closure of the water budget is verified performing the computation with a box extending in altitude up to the 300-hPa level, where outflow from the top can be considered negligible. The residual terms *Res* turned out to be always at least two orders of magnitude smaller than the others, thus providing reliability to the water budget diagnostic.

The location of the budget boxes (Fig. 1), upstream of the precipitation area, is the result of a careful analysis of the IVT and wind fields at different levels, so that the WV fluxes that exit from the northern side are mostly directed towards the region of heavy rainfall. Thus, this outflow from the box directly supplies moisture to the EPEs, and the inflow from the other three sides and from the bottom allow to identify the sources of moisture. The dimension of the boxes is the same for the two EPEs, such that the results are directly comparable, but their position is different to suitably intercept the main WV transport associated with the AR. The boxes are shown in Fig. 1, where the red box is for the 1966 flood and the orange one for Vaia.

The methodology to evaluate the contributions to the EPEs from the water budget is described in detail in Duffourg and Ducrocq, 2013 and Davolio et al., 2020a. Briefly, it consists in estimating the budget terms during a time interval whose duration corresponds to the period of intense precipitation, taking into account the temporal shift due to the time that moisture takes

to travel from the box to the precipitating system. The integration over this time interval of the lateral fluxes and of the evaporation provides the total mass (in kg) of water, mostly water vapour, belonging to different sources and all together contributing to the outflow from the northern side of the box that feeds the EPE.

2.4. RWP detection

To describe the dynamic evolution conducive to the EPEs, an analysis of RWPs and their development has been performed for both events. Global maps of the upper-tropospheric flow are produced within the latitude circles 10°N-90°N, for the day of maximum precipitation (D0), for the 6 days preceding the event (D-6, D-5, D-4, D-3, D-2, D-1) and for the following one (D+1) (Figure 2). These maps highlight the anomaly of meridional wind at 300 hPa (v'), that locates individual troughs and ridges. The envelope of the individual RWPs is then retrieved using a technique discussed in Grazzini et al., 2021, based on the original approach proposed by Zimin et al., 2003. The amplitude of the envelope is proportional to the amplitude of the RWP. The eastward movement of the envelopes in time is associated to the 'downstream development' (Wirth et al., 2018) or, in other words, the birth of new troughs and ridges on the leading edge of the packet. RWPs identification might help to recognize the cascades of dynamical processes that ultimately put in place the synoptic wave responsible for the conditions leading to the EPEs. These maps show also the 4 PVU (potential vorticity units) isolines, considering PV at 330 K: these isolines represent a measure of the waviness in the upper-tropospheric flow. PV is a fundamental quantity in the extratropics, because PV maxima anomalies at upper levels, often found as elongated filaments known as PV streamers, are able to induce cyclogenesis at the surface (Davis and Emanuel, 1991) and their magnitude is directly connected to IVT maxima and precipitation volumes (De Vries, 2021).

3. Synoptic description

In this section we describe the overall dynamical setting of the two case studies, starting from the characteristics of RWPs at synoptic scale and then moving to the mesoscale patterns. The aim is to focus on the common drivers in order to be able to isolate elements that may have contributed to the exceptional severity of these two events. At synoptic scale, both situations are associated with an amplified synoptic wave positioned over western

Europe, but their dynamical evolution and the local circulation response in the Mediterranean basin are different. The description is carried out using mainly ERA5 reanalysis data.

3.1. 1966 Flood (3 - 5 November 1966)

In the days preceding the flood, the Mediterranean basin is already influenced by the presence of a synoptic wave visible in sub panels a) to d) from (D-6 to D-3) in the left column of Fig. 2 (Full animation of the event is available in Fig. S1 of the Supplementary Material). The remaining of this cyclonic activity is reinvigorated by the arrival of a RWP initiated on 30 October (D-6) over the central Pacific (Fig. 2, a). On 1 November (D-3) an Atlantic blocking configuration is present west of UK and at 35°N a tropical depression, classified by NOAA with the name 'Lois', is developing (NOAA, 2022a). The interaction of the tropical depression with the incoming RWP produces a further amplification and a tilt of the omega-shape structure, forcing polar cold air to move southward and initiating an AR structure departing from the outflow of the tropical depression. Consequently, the trough associated with the 1966 EPE deepens over western Europe and progressively extends towards the western Mediterranean. Since the evening of 2 November and on 3 November, the AR progressively elongates from the Atlantic coast of Africa to the Mediterranean basin, making landfall over central Italy first, and then reaching the north-eastern Alps.

On 4 November the synoptic wave amplifies as the dynamical forcing from the RWP attains its maximum, as highlighted by increasing envelope values across the Atlantic (black contours in Fig. 2g). The 500 hPa geopotential isolines are almost perpendicular to the Alpine chain (Fig. 3a) and the PV streamer progressively elongates towards Italy behind the cold front (Fig. 3b). Along the front three different pressure minima develop (De Zolt et al., 2006), intensifying to 1000 hPa and reaching 994 hPa at 12 UTC. Intense precipitation occurs over the northern Apennines due to the strong orographic uplift of the moist air associated with the AR, whose IVT transport reaches a maximum intensity of about 1200 kg m^{-1} s^{-1} over the Tyrrhenian coast of central Italy at 09 UTC. Intense rainfall is also caused by deep convection (Malguzzi et al., 2006). At the same time, Sirocco winds further intensify, channeled in the Adriatic basin between the Apennines and the Dinaric Alps (Fig. 3c). This intense warm and moist flow impinging on the Alps produces a transition from 'blocked flow' to 'flow over' (Davolio et al., 2016), leading

to strong orographic lifting associated with stable or neutral conditions (Malguzzi et al., 2006). Consequently, in this phase, north-eastern Italy becomes the area affected by the heaviest precipitation.

On 5 November, another deep low pressure system develops over UK and moves southward along the Atlantic coast of the Iberian Peninsula. At the same time, the AR moves over eastern Europe followed by the trough which quickly dissipates.

3.2. Vaia Storm (27 - 30 October 2018)

Six to five days before the event, a vast ridge extends over the Atlantic, as part of a RWP already propagating to the east (sub panels a) and b) in the right column of Fig. 2) (Full animation of the event is available in Fig. S2 of the Supplementary Material). On 25 October, at D-4 (sub-panel c) the arrival of a RWP from inner US triggers a trough development in the eastern Atlantic, as also indicated by the PV undulation. This wave starts to interact with the moist flow associated with a preexisting subtropical storm (40°W, 25°N), named 'Oscar' (NOAA, 2022b), positioned further south. This interaction leads to a first explosive cyclogenesis over the east Atlantic, responsible for a strong downstream development: a trough forms over western Europe and between 26 and 27 October becomes extended from Scandinavia, over the UK and France, to the Iberian Peninsula (sub-panels d) and e). This synoptic configuration favours intense moisture advection from the eastern Atlantic Ocean to the Mediterranean, reaching northern Italy and the Alps, where the first phase of orographic precipitation, mostly stratiform, starts.

In the morning of 28 October (sub-panel f) a cut-off process begins between France and Spain, while the trough moves further south reaching northern Africa. At the surface a wide area of low pressure is present on the western Mediterranean, well in advance with respect to the upper level trough. The stationary pressure pattern leads to persistent advection of moist and warm air towards central and northern Italy. Along the eastern border of the PV streamer, an AR is well developed and transports moisture from tropical Africa across the Sahara desert to the Mediterranean. At 12 UTC on 28 October, the AR is already impinging the central Apennines, where it is responsible for heavy precipitation (Davolio et al., 2020a).

In the second half of the day the trough axis starts to rotate counterclockwise and becomes meridionally oriented. On 29 October the trough slowly

moves eastward increasing the meridional moisture transport associated with the AR.

On 29 October, another weaker RWP is propagating across the Atlantic, leading to a new Atlantic east coast cyclogenesis, which in turn reinforces the downstream trough over the Mediterranean (sub-panel g). At the surface, the advection of cold air of Mistral from the Gulf of Lion (Fig. 4c), combined with the warm anomaly of SSTs on the western Mediterranean (Davolio et al., 2020a), produces strong baroclinicity that, associated with an intense upper tropospheric forcing (Fig. 4b), is responsible for the explosive Mediterranean cyclogenesis: the surface low shows a rapid deepening reaching 977 hPa at 18 UTC of 29 October (Giovannini et al., 2021). The pressure drop, combined with the rotation of the trough axis, leads to a further intensification of the AR (IVT $\sim$ 1200 kg m^{-1} s^{-1}), which is bent back and again impinges on the eastern Italian Alps (Fig. 4a). The final phase of precipitation is associated with the passage of the cold front and is also characterized by convective activity. Finally, on 30 October the trough and the AR move eastward, overtaking Italy and leaving the Mediterranean.

3.3. Comparison between the two events

The two EPEs show many similarities. First of all, they are temporally located in the same period of the year between the end of October and the beginning of November. This is in line with the results of Grazzini et al., 2020, who showed that the peak of the seasonal distribution of EPEs in Italy is in autumn, when the SST is high enough to provide a considerable source of moisture and to create strong thermal contrasts when cold air outbreaks are able to penetrate in the Mediterranean basin. Moreover, the two EPEs have a similar synoptic development, compatible with the fact that they both belong to the same Cat 2 classification by Grazzini et al., 2021. The evolution of both events is connected to the advance and amplification of a baroclinic wave that slowly propagates eastward. A trough deepens over western Europe and moves over the western Mediterranean; at the surface strong Sirocco winds are channeled along the Adriatic Sea towards north-eastern Italy. Finally, a cold front sweeps over Italy, leading to high rates of precipitation and intense convection. Moreover, in both events a tropical depression is present in the subtropical Atlantic region: respectively 'Lois' for the 1966 flood and the subtropical storm 'Oscar' for Vaia. These tropical depressions are connected to the formation phase of the ARs and thus are likely to have contributed to the transport of WV towards Europe.

The analysis of Fig. 2 shows that both synoptic waves are initiated by short-lived RWPs propagating from the western American coast. On the other hand, the final amplification of the wave is due to the action of a second and faster RWP propagating over longer distances from the eastern Pacific, moving across the US continent and reaching Europe after the first RWP. It is worth noticing that the quasi-stationarity and a further amplification of a pre-existent trough are often observed at the end of the Atlantic storm track, in conjunction with persistent extreme weather over Europe. It occurs due to a sequence of incoming RWPs, with the group velocity of the following RWP usually higher than the first, leading to a constructive interference. In favourable conditions this produces a recurrent amplification (a sort of resonance) of troughs and ridges at the same longitudes, as shown by Barton et al., 2016 and Röthlisberger et al., 2019. This is compatible with the fact that during the transition season the storm track progressively intensifies, with an increasingly stronger wave-guiding. This makes these phenomena more likely during this transient phase.

From the ArCIS database it is possible to evaluate the spatial distribution of accumulated precipitation over the whole events. Figure 5a shows the accumulated rainfall in 48 hours from 08 UTC, 03 November, to 08 UTC, 05 November 1966. The most affected areas are north-eastern Italy (Friuli-Venezia Giulia and partly Veneto regions), with a peak of 635 mm, and Tuscany, where local peaks attain values higher than 350 mm. For the Vaia case (Fig. 5b), the accumulated precipitation in 72 hours from 00 UTC, 27 October, to 00 UTC, 30 October 2018 shows high amounts over Liguria (>500 mm) and over the whole Alpine chain, with local peaks at the border between Friuli-Venezia Giulia and Veneto regions (425 mm), at the border between Veneto and Trentino-Alto Adige (>500 mm) and in Piedmont at the border with Switzerland (>450 mm). Therefore, it is evident that the spatial distribution of precipitation is considerably different in the two events, that share only the highest values of rainfall over north-eastern Italy. In more details, in the 1966 event, rainfall maxima are clearly oriented in an almost meridional direction from Tuscany to the north-eastern Alps. Vaia, instead, shows heavy precipitation spread all over the Alpine chain and Liguria. This pattern is due to the different characteristics of the ARs, as will be explained in Section 4.1.

The comparison between the precipitation distribution in the two events also highlights that the overall amount of rainfall is higher during Vaia. To quantify this aspect, the total volume of water accumulated over the ArCIS

domain is calculated. It results in $18.0 \cdot 10^9$ m^3 for the 1966 flood and $20.5 \cdot 10^9$ m^3 for Vaia. However, it is important to remember that these values do not refer to the same time period, due to the different duration of the two EPEs: 3 days for Vaia and 2 days for the 1966 flood.

4. Numerical experiments

The BOLAM model is used to simulate higher resolution details (in space and time) of the two EPEs and to perform the water budget study. The reliability of the simulations is verified comparing the numerical results with observations, especially the cumulated precipitation from the ArCIS database shown in Fig. 5. Simulations obtained from BOLAM well reproduce the locations of the maxima, but show an overall underestimation of the observed cumulated precipitation, particularly of the local maxima (not shown). However, the results can be considered satisfactory and suitable for the purposes of this study, since they reproduce with enough accuracy the dynamical evolution of the two events.

4.1. Atmospheric rivers

In the development phase of the ARs (3 November for 1966 flood and 27 October for Vaia), IVT maps from ERA5 data (not shown) show that the AR in the 1966 flood is longer and broader, extending in longitude from 50°W to 10°E and in latitude from 20°N to 45°N (longer than 8000 km), reaching a maximum IVT value of approximately 1200 kg m^{-1} s^{-1}. On the other hand, the AR during Vaia is narrower and never extends west of 20°W (slightly longer than 6000 km). In both cases, in the early stage there is a very intense IVT connected with the tropical depressions, as described in Section 3.3, and showed in Fig. 3a and Fig. 4a. In particular, in the 1966 flood the AR is wrapped around the tropical depression and seems to draw WV from that source. In Vaia there is a net substantial transport coming from the subtropical storm, even if there is not a clear unique filament linking 'Oscar' to the main AR structure.

The features shown in the development phase significantly change looking at the ARs in the phase of maximum IVT, which corresponds approximately to 4 November 1966 at 06 UTC for the 1966 flood and 29 October 2018 at 12 UTC for Vaia. BOLAM simulations (Fig. 6) show that the IVT magnitude over the Mediterranean region is stronger in Vaia with respect to the 1966 flood. Moreover, the AR in Vaia is broader over the Tyrrhenian Sea and

changes its position, being bent back during the last day, thus leading to a more widespread distribution of the transported WV all over northern Italy. The AR in the 1966 flood, instead, is narrower and the axis does not change its orientation during the whole event, thus focusing the transport over Tuscany and north-eastern Italy. These features of the ARs explain the different spatial distribution of the precipitation found in the two EPEs and discussed in Section 3.3.

To evaluate the vertical structure of the ARs and to investigate the WV transport at different heights (and not only in a vertically integrated perspective through IVT) Fig. 7 shows a cross section (whose location is shown in Fig. 1) of the WV flux and of the meridional component of the wind in correspondence to the period of maximum intensity of the ARs. The ARs show a similar vertical extension up to 600 hPa and also similar maximum values of WV flux and meridional wind speed, located around the 800 hPa level. However, they reveal significant differences in the zonal extension: while in 1966 the AR is confined only over the Tyrrhenian Sea, west of the Apennines (Fig. 7a), in Vaia the WV flux maximum covers the whole region between Corsica and the Apennines and also the area over the Adriatic Sea (Fig. 7b). Therefore, although the AR in the 1966 flood is longer and draws moisture from a more distant source, in the phase of maximum WV transport over the Mediterranean the AR in Vaia is clearly broader and more intense.

4.2. Water budget: 1966 flood (3 - 5 November 1966)

The evolution of the event is here discussed by taking advantage of the hourly cumulated precipitation histogram over northern Italy (the investigated area is shown in Fig. 1) and of the water budget introduced in Section 2.3. Fig. 8a clearly shows that the 1966 flood was characterized by a single precipitation phase with an approximately constant rain rate from 3 November 18 UTC to 4 November 18 UTC. This high constant rate for almost 24 hours is likely due to the persistence of the AR in the same position, as highlighted in Section 4.1.

The water budget computed up to 700 hPa (Fig. 8b) is suitable to provide information about the AR contribution that, as previously shown, is mainly confined under this pressure level. Figure 8b only shows the most relevant components of the water budget of Eq. 1, i.e. the lateral fluxes and the evaporation from the sea.

As expected, the evolution of FN and of the rainfall over northern Italy are strictly connected. The maximum value of FN is followed by the maximum

precipitation intensity and the delay simply represents the time the WV needs to be advected from the box boundary to the Alpine area. The outgoing flux is generated by several contributions in the box. The flux entering from the southern side (FS) is the dominant term, being associated to the strong WV transport of the AR. The AR partly enters also from the western side (FW). It is worth noting that also FE is positive and relevant for almost 24 hours since the afternoon of 03 November. This feature can be explained by analyzing the IVT map in Fig. 6a, showing the WV transport on 4 November at 6 UTC, when FE has a positive value. It is evident a north-westward transport of moisture into the box coming from the eastern Mediterranean and directed towards southern Italy. This WV transport is especially confined in the lower troposphere and it peaks below the 850 hPa level. This moist current does not show connection with remote sources of WV far to the east, but it has an almost local origin, since it is likely due to evaporation from the eastern Mediterranean Sea surface. The WV contribution coming from the sea surface beneath an AR is often negligible, due to the saturation of the lower levels that inhibits further evaporation (Ralph et al., 2020). In this case, instead, the local contribution is efficient because the evaporation comes not only from the area below the AR within the analysis box, but also from a region that is very close, but outside the AR track.

After 4 November at 17 UTC both FS and FE drop and become negative, due to the passage of the cold front. FW remains positive since the post-frontal wind is directed perpendicular to the cold front, i.e. eastward. Consequently, also the outgoing flux quickly decreases and the rainfall weakens.

4.3. Water budget: Vaia storm (27 - 30 October 2018)

The precipitation histogram for the Vaia storm (Fig. 9a) shows two precipitation phases. The first phase starts on 27 November at 06 UTC and ends on 28 November at 18 UTC, followed by a 12 hours period with reduced precipitation that was dramatically important to prevent extensive flooding, since it allowed a temporary but substantial decrease of river discharges. The second phase, which is shorter but more intense, develops between 29 October at 06 UTC and 30 October at 00 UTC. According to this evolution, the analysis of the water budget is performed separating the two different phases.

From the water budget computed up to 700 hPa (Fig. 9b), the outgoing flux shows two peaks, each of them well correlated with the maximum

intensity of rainfall. Concerning ingoing contributions, the surface evaporation results almost constant from 26 to 29 October, with an average value of $0.31 \cdot 10^8$ kg s^{-1} (slightly less than in 1966). From 29 October at 06 UTC, there is an increasing trend in evaporation when the cold front enters in the box. In fact, the strong winds just ahead of the cold front over the Mediterranean Sea favour surface evaporation, which is also fostered by the advection of cold and dry air behind the front, that removes the supersaturation layer above the surface. Contrarily to the 1966 flood budget, FE has not a dominant role and it is almost always small and negative.

The budget indicates that the first phase of precipitation is not related to the AR. Specifically, as discussed in Davolio et al., 2020a, the high values of FW, with respect to FS, reveal a stream of moisture entering the Mediterranean from the Atlantic and moving towards the Alps. The AR core, instead, in this phase is still localized over northern Africa and starts approaching the box on its south-western side. Therefore, differently from the 1966 case, in Vaia there is a contribution from the Atlantic that does not belong to the AR. Therefore, both FW and FS are related to a remote transport of WV, but coming from different sources.

The second phase of precipitation is effectively caused by the arrival of the AR over the Italian territory. In this phase FS dominates the atmospheric water budget and it is entirely connected to the tropical transport. Later, the increase of FS is also related to the cold front that organizes low-level WV transport ahead of it, across the southern side of the box.

4.4. Water supply to the EPEs and comparison

The different contributions to the two EPEs presented in Figs. 8b and 9b are integrated in time and quantitatively evaluated, following the methodology described in Section 2.3. The relative contribution of each flux to the overall mass of water entering into the box are presented in Table 1. The percentages reported have to be interpreted as the relative contribution of each specific flux to the whole water mass that feeds precipitation over northern Italy.

In the 1966 event the contribution across the southern side dominates the budget, confirming the importance of the transport due to the AR. The relative role of FE in the 1966 flood is significantly more relevant than in Vaia. As discussed in Section 4.2, this can be considered as a local contribution, due to the evaporation from the near eastern Mediterranean.

FLUX	1966 flood	Vaia 1st phase	Vaia 2nd phase
South Flux (FS)	42%	39%	59%
West Flux (FW)	21%	47%	22%
East Flux (FE)	21%	0%	4%
Evaporation (E)	14%	13%	13%

Table 1: Percentage contributions related to the water mass entering the box from each lateral flux and evaporation with respect to the overall entering water mass (FW+FS+FE+E).

The first phase of the Vaia storm is the only one characterized by a predominance of the westerly contribution FW. In fact, before the arrival of the AR, the advection from the northern Atlantic plays an important role.

The second phase of Vaia shows the overwhelming preponderance of FS, that reaches almost 60%, confirming that the broad and intense AR is responsible for most of the WV transport. Therefore, the contribution from remote sources is substantial.

The evaporation from the sea surface contributes to approximately 13% of the budget both in the 1966 flood and in the two phases of Vaia. In fact, evaporation in both EPEs is an almost constant process over the whole time period. Although this percentage seems to indicate a negligible effect of evaporation, a correct and more complex interpretation is required to assess the role of local and remote sources. Actually, lateral fluxes are related to advection from remote regions and they are the result of the collection of WV over large areas, in a long period and over the whole vertical extension of the atmosphere. Evaporation, instead, is a local process that is evaluated only over the base area of the box and in a time window over which the AR tends to saturate the lower atmospheric levels. However, evaporation provides moisture all over the Mediterranean basin also in the days before the event, that is then advected across the box and converges in the AR transport. We have considered the transport from the eastern Mediterranean in the 1966 event as evaporation, but it is not always simple to trace the moisture coming from the sea surface. All in all, it means that possibly the role of evaporation is somehow underestimated by this methodology. Finally, it is also important to recall that sea surface fluxes may modify vertical atmospheric profiles in the planetary boundary layer, and this is relevant especially when air masses interact with orography to produce heavy precipitation, as shown in Stocchi and Davolio, 2017 and Davolio et al., 2017.

5. Conclusions

The 1966 flood (3-5 November 1966) and the Vaia storm (27-30 October 2018) are the two most severe precipitation events occurred over northern and central Italy since 1961. They are compared in this study with the aim of highlighting similarities and differences using reanalysis (ERA5), observational data (ArCIS dataset), as well as numerical simulations (BOLAM).

The two EPEs share a similar large-scale configuration, which is typical of this type of events over northern Italy during autumn. They are the result of a vigorous amplification of a baroclinic wave extending over the western Mediterranean and slowly evolving eastward, which favors the meridional transport of moisture. This critical amplification, in both cases, is related to the synergy of two incoming RWPs merging over the Atlantic and reinforcing the downstream development of the cyclonic circulation over the Mediterranean Sea. Cyclogenesis occurs at the surface in both events over the western Mediterranean Sea; however, the Vaia storm is characterized by an explosive intensification of the surface cyclone of 20 hPa in 18 h up to 977 hPa (Davolio et al., 2020a), with respect to the 994 hPa measured for the 1966 event (Malguzzi et al., 2006). The peculiar value of mean sea level pressure reached in Vaia highlights the stronger baroclinicity of the environment and the combination with a vigorous upper level forcing (jet stream) suitably located with respect to the surface pressure minimum.

In terms of impacts at the ground, the two events reveal a similar amount of total precipitation volume over north-central Italy, although in 1966 the duration is shorter and the spatial distribution is very different, except than over the north-eastern Italian Alps. Here, the precipitation is mainly of orographic nature, associated with uplift of warm, moist and gusty Sirocco winds near the surface, driven by the strong zonal pressure gradient and channelled between the Apennines and the Dinaric Alps. Also intense convection, especially in specific phases of the events, is embedded in the orographic rainfall. However, in both EPEs a significant amount of water vapour is transported by the ARs from tropical regions into the Mediterranean basin. Therefore, the characteristics of the ARs and their evolution explain most of the observed spatial precipitation patterns. The AR in Vaia is more intense and broader, and its axis oscillates back and forth over the Tyrrhenian Sea, thus spreading the WV transport over a wider area. This in turn produces precipitation all over northern Italy, with maximum intensity over the north-eastern Alps and Liguria region. The AR in the 1966 flood is longer and narrower,

thus transporting water vapour from even farther tropical areas. However, once over the Mediterranean basin, its axis steadily remains meridionally oriented towards Tuscany and north-eastern Italy, thus leading to a localized spatial pattern of precipitation that closely follows this direction. The AR during Vaia attains higher IVT values. However, to compare the effect of different ARs, the magnitude of the IVT is not the only important variable to consider. In particular, as discussed in Ralph et al., 2019, the duration is a critical factor as well. From this perspective the AR in the 1966 flood persists in the same position for almost 18 hours, while in the Vaia storm the more complex dynamical development leads to a less steady behavior of the AR. Therefore, the associated water transport does not constantly impinge on the same position of the Alpine chain for the whole duration of the event.

A water budget computation is performed to evaluate the main contributing fluxes and disentangle local sources of WV (i.e. evaporation from the Mediterranean Sea) from transport from remote areas. The results show that in both EPEs the southerly WV transport is the dominant contribution, highlighting the key role of the ARs in the moisture supply to the precipitation systems. Moreover, in the 1966 flood a local westward transport in the lower layers, coming from the eastern Mediterranean, significantly contributes to the event: the local origin of this flux has to be mainly ascribed to the evaporation from the sea surface in nearby areas. Instead, the Vaia event is mainly characterized by remote transport of WV coming from two different sources: a contribution from the North Atlantic, that is crucial in the first precipitation phase, and a southerly transport of tropical origin later on. The evaporation from the sea surface below the AR track in both events seems to play a minor but not negligible role.

The ARs explain the spatial precipitation patterns and result as key ingredients for the observed extreme rainfall; however, they are not the only relevant factor. In particular, it is important to mention the contribution of Sirocco winds to provide additional WV from the Adriatic basin, which is not evaluated through the water budget technique adopted. Maps of 1000 hPa wind over the Adriatic Sea show that, despite the severe damages due to wind gusts in Vaia, the Sirocco winds are stronger offshore in 1966 and also much more persistent. In fact, in 1966 the Sirocco blows towards the Alpine chain for almost the entire duration of the precipitation event (36 hours), while in Vaia storm the wind is mainly southerly at the beginning of the event and turns into south-easterly Sirocco only on 29 October. This means that in the lower layers affected by this moist flow from the Adriatic

basin, WV is transported in larger amount during the 1966 flood and this partially compensates the lower overall intensity of the AR. Together with the stationarity of the AR, this explains the extreme values of precipitation recorded in only 48 hours over the north-eastern Italian Alps in 1966. Finally, as already mentioned in the Introduction, the damages due to precipitation in the two events have to be related to the meteorological conditions before the development of the events: Vaia came after a dry period while 1966 flood happened after a series of precipitation episodes and this drastically changed the hydrological situation in terms of saturated conditions of soils and river discharge. Moreover, the hiatus of precipitation between the two phases in Vaia likely prevented much more adverse impacts (Giovannini et al., 2021).

In conclusion, this work highlights the connection between EPEs and the magnitude of WV transport by ARs. This work definitely sheds light on the synoptic configuration that leads to the most severe EPEs over northern Italy in autumn (October-November). EPEs are expected to significantly increase due to climate change in the next decades (Donat et al., 2016; Giorgi et al., 2019; Tramblay and Somot, 2018; Zittis et al., 2021). Consequently, providing the forecasters with the necessary elements to identify in advance evidences of EPEs, through the prediction of the key precursors, is of fundamental importance in terms of civil protection and damage confinement.

6. References

AMS, 2022. Glossary of meteorology: definition of atmospheric river. https://glossary.ametsoc.org/wiki/Atmospheric_river#:~:text=A%20long%2C%20narrow%2C%20and%20transient,and%2For%20extratropical%20moisture%20sources., [Online; accessed 20-July-2022].

Antolini, G., Auteri, L., Pavan, V., Tomei, F., Tomozeiu, R., Marletto, V., 2016. A daily high-resolution gridded climatic data set for Emilia-Romagna, Italy, during 1961-2010. International Journal of Climatology 36 (4), 1970–1986.

Barton, Y., Giannakaki, P., Von Waldow, H., Chevalier, C., Pfahl, S., Martius, O., 2016. Clustering of regional-scale extreme precipitation events in southern Switzerland. Monthly Weather Review 144 (1), 347–369.

Berto, A., Buzzi, A., Zardi, D., 2005. A warm conveyor belt mechanism accompanying extreme precipitation events over north-eastern Italy. Hrvatski meteorološki časopis 40 (40), 338–341.

Buzzi, A., Davolio, S., Malguzzi, P., Drofa, O., Mastrangelo, D., 2014. Heavy rainfall episodes over Liguria in autumn 2011: numerical forecasting experiments. Natural Hazards and Earth System Sciences 14 (5), 1325–1340.

Buzzi, A., Fantini, M., Malguzzi, P., Nerozzi, F., 1994. Validation of a limited area model in cases of Mediterranean cyclogenesis: surface fields and precipitation scores. Meteorology and Atmospheric Physics 53 (3), 137–153.

Capecchi, V., Buizza, R., 2019. Reforecasting the flooding of Florence of 4 November 1966 with global and regional ensembles. Journal of Geophysical Research: Atmospheres 124 (7), 3743–3764.

Cavaleri, L., Bajo, M., Barbariol, F., Bastianini, M., Benetazzo, A., Bertotti, L., Chiggiato, J., Davolio, S., Ferrarin, C., Magnusson, L., Others, 2019. The October 29, 2018 storm in Northern Italy–an exceptional event and its modeling. Progress in oceanography 178, 102–178.

Davis, C. A., Emanuel, K. A., 1991. Potential vorticity diagnostics of cyclogenesis. Monthly weather review 119 (8), 1929–1953.

Davolio, S., Della Fera, S., Laviola, S., Miglietta, M. M., Levizzani, V., 2020a. Heavy precipitation over Italy from the Mediterranean storm Vaia in October 2018: Assessing the role of an atmospheric river. Monthly Weather Review 148 (9), 3571–3588.

Davolio, S., Henin, R., Stocchi, P., Buzzi, A., 2017. Bora wind and heavy persistent precipitation: atmospheric water balance and role of air-sea fluxes over the Adriatic Sea. Quarterly Journal of the Royal Meteorological Society 143 (703), 1165–1177.

Davolio, S., Malguzzi, P., Drofa, O., Mastrangelo, D., Buzzi, A., 2020b. The Piedmont flood of November 1994: A testbed of forecasting capabilities of the CNR-ISAC meteorological model suite. Bulletin of Atmospheric Science and Technology 1 (3), 263–282.

Davolio, S., Volonté, A., Manzato, A., Pucillo, A., Cicogna, A., Ferrario, M. E., 2016. Mechanisms producing different precipitation patterns over

north-eastern Italy: insights from HyMeX-SOP1 and previous events. Quarterly Journal of the Royal Meteorological Society 142, 188–205.

De Vries, A. J., 2021. A global climatological perspective on the importance of Rossby wave breaking and intense moisture transport for extreme precipitation events. Weather and Climate Dynamics 2 (1), 129–161.

De Zolt, S., Lionello, P., Nuhu, A., Tomasin, A., 2006. The disastrous storm of 4 November 1966 on Italy. Natural Hazards and Earth System Sciences 6 (5), 861–879.

Donat, M. G., Lowry, A. L., Alexander, L. V., O'Gorman, P. A., Maher, N., 2016. More extreme precipitation in the world's dry and wet regions. Nature Climate Change 6 (5), 508–513.

Done, J. M., Craig, G. C., Gray, S. L., Clark, P. A., Gray, M. E. B., 2006. Mesoscale simulations of organized convection: Importance of convective equilibrium. Quarterly Journal of the Royal Meteorological Society 132 (616), 737–756.

Duffourg, F., Ducrocq, V., 2013. Assessment of the water supply to Mediterranean heavy precipitation: a method based on finely designed water budgets. Atmospheric Science Letters 14 (3), 133–138.

Gimeno, L., Nieto, R., Vázquez, M., Lavers, D. A., 2014. Atmospheric rivers: A mini-review. Frontiers in Earth Science 2, 2.

Giorgi, F., Raffaele, F., Coppola, E., 2019. The response of precipitation characteristics to global warming from climate projections. Earth System Dynamics 10 (1), 73–89.

Giovannini, L., Davolio, S., Zaramella, M., Zardi, D., Borga, M., 2021. Multimodel convection-resolving simulations of the October 2018 Vaia storm over Northeastern Italy. Atmospheric Research 253, 105455.

Grazzini, F., Craig, G. C., Keil, C., Antolini, G., Pavan, V., 2020. Extreme precipitation events over northern Italy. Part I: A systematic classification with machine-learning techniques. Quarterly Journal of the Royal Meteorological Society 146 (726), 69–85.

Grazzini, F., Fragkoulidis, G., Teubler, F., Wirth, V., Craig, G. C., 2021. Extreme precipitation events over northern Italy. Part II: Dynamical precursors. Quarterly Journal of the Royal Meteorological Society 147 (735), 1237–1257.

Hersbach, H., Bell, B., Berrisford, P., Hirahara, S., Horányi, A., Muñoz-Sabater, J., Nicolas, J., Peubey, C., Radu, R., Schepers, D., Others, 2020. The ERA5 global reanalysis. Quarterly Journal of the Royal Meteorological Society 146 (730), 1999–2049.

Hoskins, B. J., Ambrizzi, T., 1993. Rossby wave propagation on a realistic longitudinally varying flow. Journal of Atmospheric Sciences 50 (12), 1661–1671.

Kain, J. S., 2004. The Kain–Fritsch convective parameterization: an update. Journal of applied meteorology 43 (1), 170–181.

Krichak, S. O., Barkan, J., Breitgand, J. S., Gualdi, S., Feldstein, S. B., 2015. The role of the export of tropical moisture into midlatitudes for extreme precipitation events in the Mediterranean region. Theoretical and Applied Climatology 121 (3), 499–515.

Lorenz, E. N., 1972. Barotropic instability of Rossby wave motion. Journal of Atmospheric Sciences 29 (2), 258–265.

Malguzzi, P., Grossi, G., Buzzi, A., Ranzi, R., Buizza, R., 2006. The 1966 century flood in Italy: A meteorological and hydrological revisitation. Journal of Geophysical Research: Atmospheres 111 (D24).

Morcrette, J. J., Barker, H. W., Cole, J. N. S., Iacono, M. J., Pincus, R., 2008. Impact of a new radiation package, McRad, in the ECMWF Integrated Forecasting System. Monthly weather review 136 (12), 4773–4798.

Motta, R., Ascoli, D., Corona, P., Marchetti, M., Vacchiano, G., 2018. Selvicoltura e schianti da vento: il caso della tempesta Vaia. Forest Rivista di Selvicoltura ed Ecologia Forestale.

Myhre, G., Alterskjær, K., Stjern, C. W., Hodnebrog, Ø., Marelle, L., Samset, B. H., Sillmann, J., Schaller, N., Fischer, E., Schulz, M., Others, 2019. Frequency of extreme precipitation increases extensively with event rareness under global warming. Scientific reports 9 (1), 1–10.

NOAA, 2022a. Historical hurricane tracks for 1966 year. https://www.nhc.noaa.gov/data/tracks/tracks-at-1966.png, [Online; accessed 20-July-2022].

NOAA, 2022b. Historical hurricane tracks for 2018 year. https://www.nhc.noaa.gov/data/tracks/tracks-at-2018.png, [Online; accessed 20-July-2022].

Pavan, V., Antolini, G., Barbiero, R., Berni, N., Brunier, F., Cacciamani, C., Cagnati, A., Cazzuli, O., Cicogna, A., De Luigi, C., Others, 2019. High resolution climate precipitation analysis for north-central Italy, 1961–2015. Climate Dynamics 52 (5), 3435–3453.

Ralph, F. M., Dettinger, M. D., Rutz, J. J., Waliser, D. E., 2020. Atmospheric rivers. Vol. 1. Springer.

Ralph, F. M., Rutz, J. J., Cordeira, J. M., Dettinger, M., Anderson, M., Reynolds, D., Schick, L. J., Smallcomb, C., 2019. A scale to characterize the strength and impacts of atmospheric rivers. Bulletin of the American Meteorological Society 100 (2), 269–289.

Raveh-Rubin, S., Flaounas, E., 2017. A dynamical link between deep Atlantic extratropical cyclones and intense Mediterranean cyclones. Atmospheric Science Letters 18 (5), 215–221.

Ritter, B., Geleyn, J.-F., 1992. A comprehensive radiation scheme for numerical weather prediction models with potential applications in climate simulations. Monthly weather review 120 (2), 303–325.

Röthlisberger, M., Frossard, L., Bosart, L. F., Keyser, D., Martius, O., 2019. Recurrent synoptic-scale Rossby wave patterns and their effect on the persistence of cold and hot spells. Journal of Climate 32 (11), 3207–3226.

Stocchi, P., Davolio, S., 2017. Intense air-sea exchanges and heavy orographic precipitation over Italy: The role of Adriatic sea surface temperature uncertainty. Atmospheric Research 196, 62–82.

Tramblay, Y., Somot, S., 2018. Future evolution of extreme precipitation in the Mediterranean. Climatic Change 151 (2), 289–302.

Wirth, V., Riemer, M., Chang, E., Martius, O., 2018. Rossby Wave Packets on the Midlatitude Waveguide : A Review. Monthly Weather Review 146.

Zampieri, M., Malguzzi, P., Buzzi, A., 2005. Sensitivity of quantitative precipitation forecasts to boundary layer parameterization: a flash flood case study in the Western Mediterranean. Natural Hazards and Earth System Sciences 5 (4), 603–612.

Zimin, A. V., Szunyogh, I., Patil, D. J., Hunt, B. R., Ott, E., 2003. Extracting envelopes of Rossby wave packets. Monthly weather review 131 (5), 1011–1017.

Zittis, G., Bruggeman, A., Lelieveld, J., 2021. Revisiting future extreme precipitation trends in the Mediterranean. Weather and climate extremes 34, 100380.

7. Figures

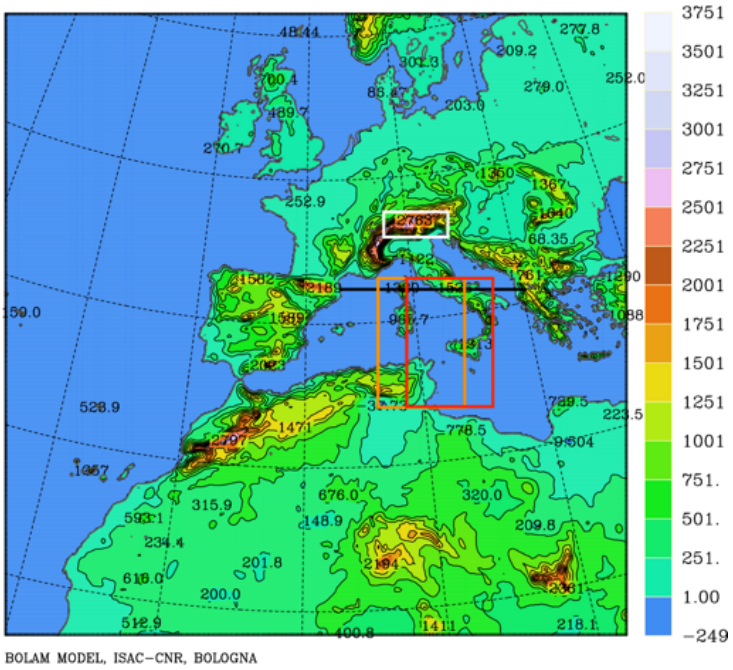

Figure 1: BOLAM integration domain and model orography. The red (orange) box indicates the location of the budget box for the 1966 flood (Vaia storm). The black line shows the position of the cross section shown in Fig. 7. The white box is the area over which precipitation histograms are computed.

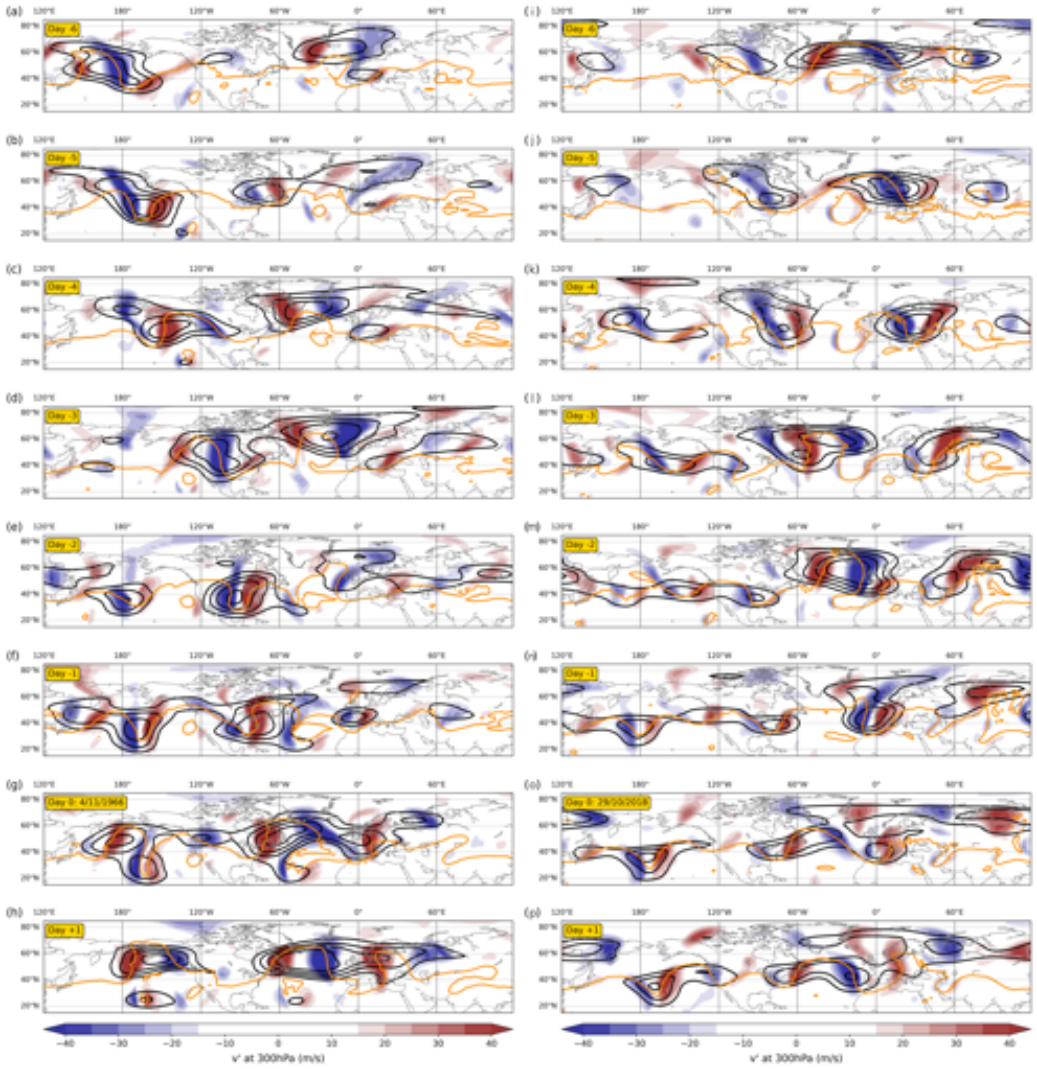

Figure 2: Evolution of the upper-tropospheric flow leading to the EPEs: 1966 flood (subpanels a-g), Vaia storm (subpanels i-p). The panels depict data of ERA5 reanalysis: mean daily values of v' at 300 hPa (colours), the corresponding envelope at 300 hPa (black contours every 10 m s^{-1} starting from 25 m s^{-1}) and the 4 PVU isoline at 330 K (orange contour) on the day of maximum precipitation D0 (4 November 1966 for 1966 flood and 29 October 2018 for Vaia storm), the 6 days preceding the event (D-6, D-5, D-4, D-3, D-2, D-1) and the following day (D+1). Data are related to 12 UTC. Courtesy of Georgios Fragkoulidis (Johannes Gutenberg-University, Mainz).

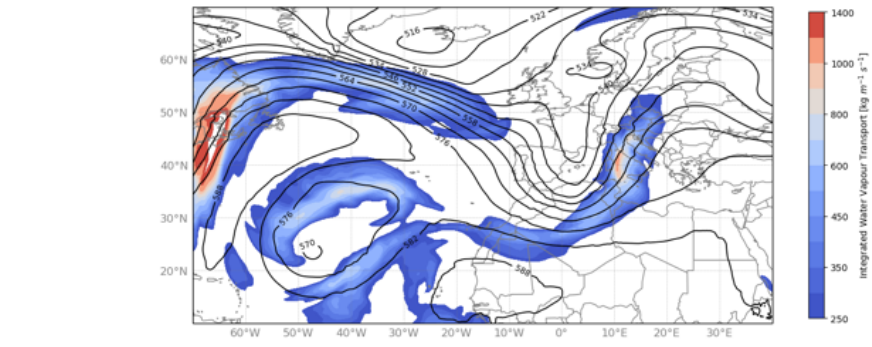

(a)

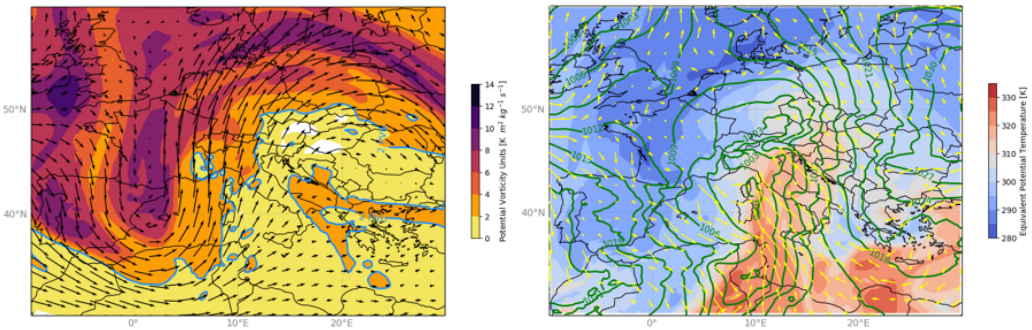

(b) (c)

Figure 3: 1966 flood: ERA5 reanalysis maps on 4 Nov. 1966, 00 UTC. (a) Geopotential height at 500 hPa (contours) and IVT (colours), (b) PV at 330 K and wind at 300 hPa, (c) equivalent potential temperature (colours), mean sea level pressure (contours) and wind at 1000 hPa.

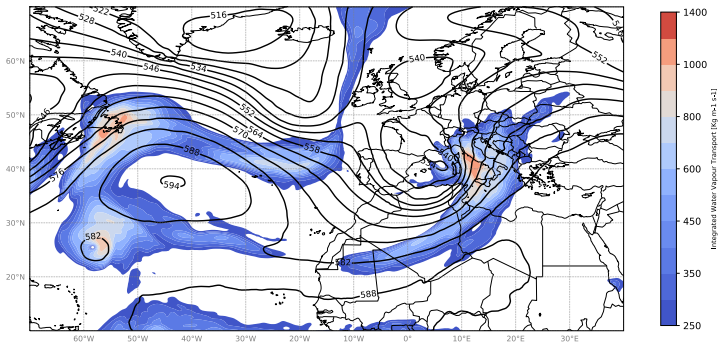

(a)

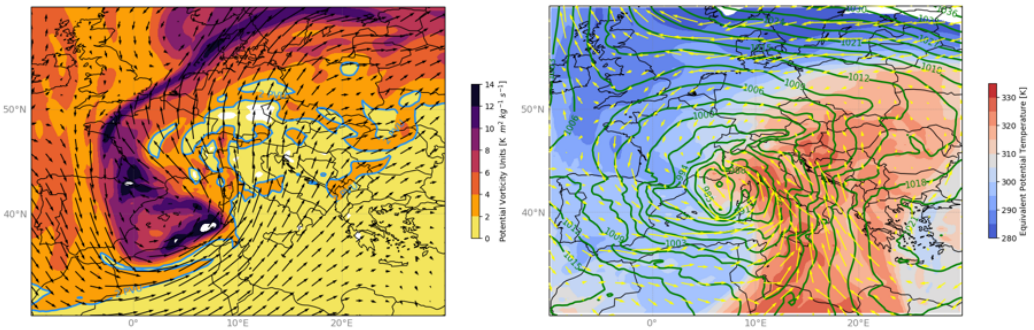

(b) (c)

Figure 4: As in Fig. 3 but for the Vaia storm on 29 Oct. 2018, 12 UTC.

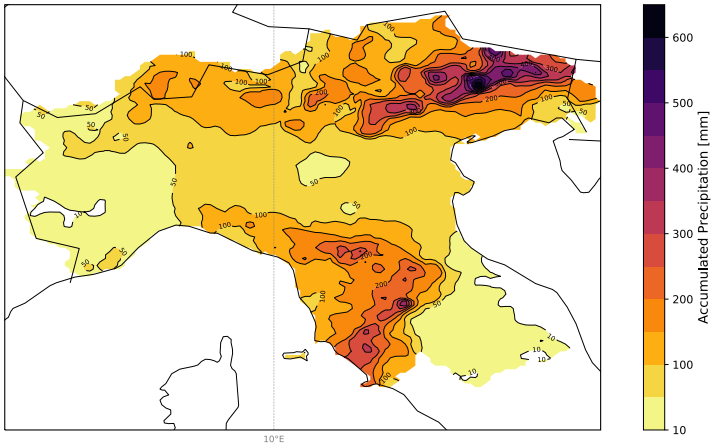

(a)

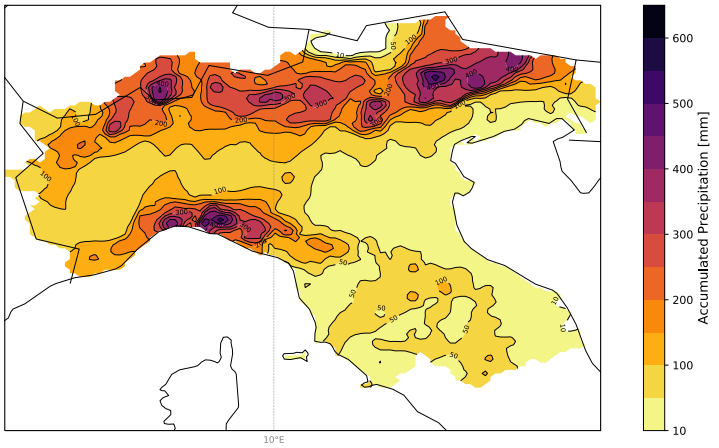

(b)

Figure 5: Accumulated precipitation from ArCIS database. (a) 1966 flood: from 3 Nov., 08 UTC, to 5 Nov., 8 UTC (b) Vaia storm: from 27 Oct., 00 UTC, to 30 Oct. 2018, 00 UTC.

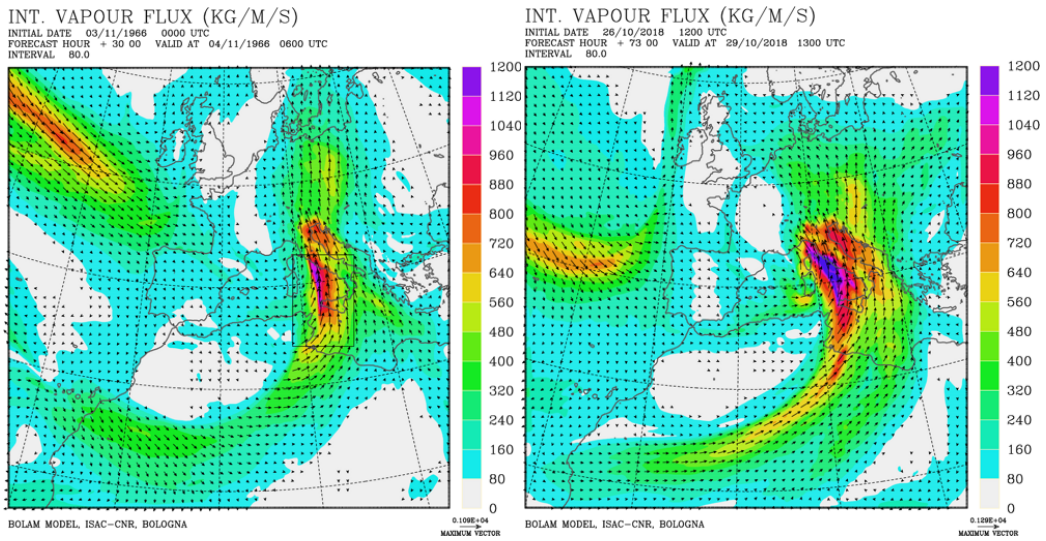

(a) (b)

Figure 6: IVT field integrated up to 300 hPa, at the time corresponding to the maximum AR intensity for (a) 1966 flood (4 Nov. 1966, 06 UTC) and (b) Vaia storm (29 Oct. 2018, 13 UTC).

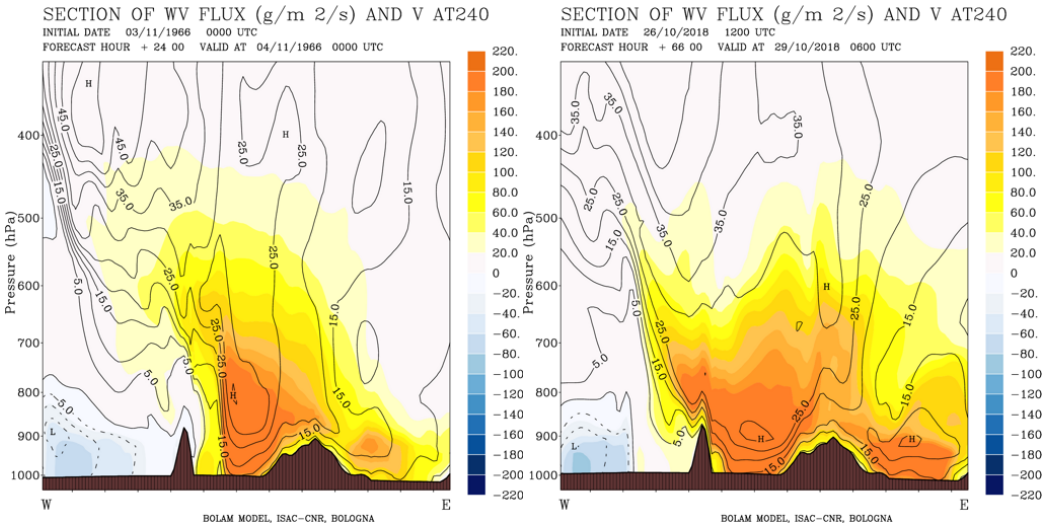

(a) (b)

Figure 7: Vertical cross sections of the normal components of water vapour flux (g m^{-2} s^{-1}; color shading) and wind (m s^{-1}; contour lines every 5 m s^{-1}) for (a) 1966 flood (4 Nov. 1966, 00 UTC) and (b) Vaia storm (29 Oct. 2018, 06 UTC). The location of the section is displayed in Fig. 1.

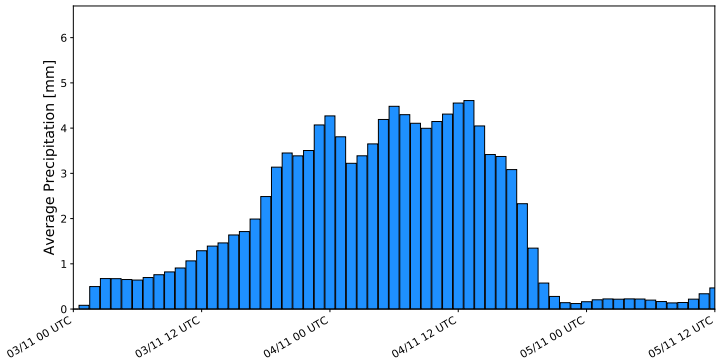

(a)

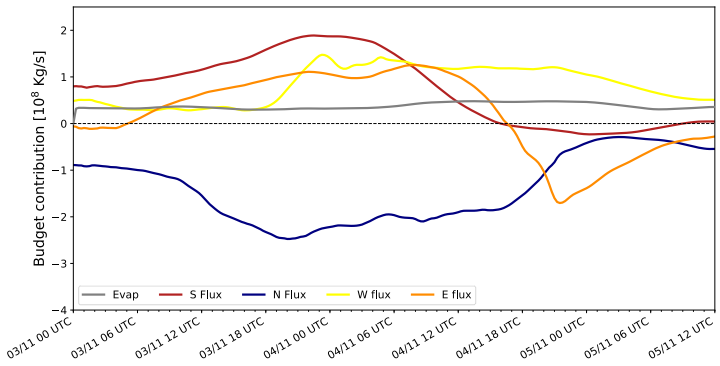

(b)

Figure 8: 1966 flood: (a) Area-averaged hourly accumulated precipitation per cell over northern Italy; (b) evolution of the atmospheric water budget computed up to 700 hPa.

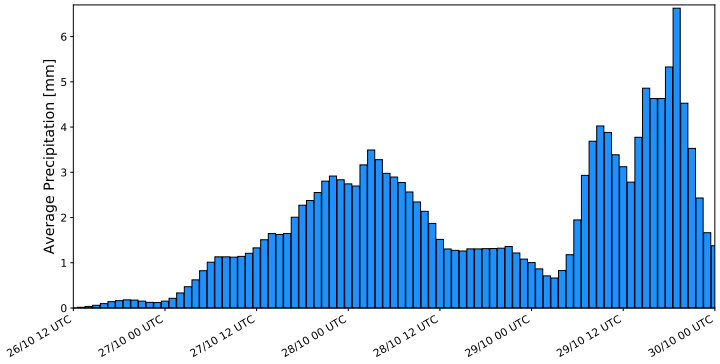

(a)

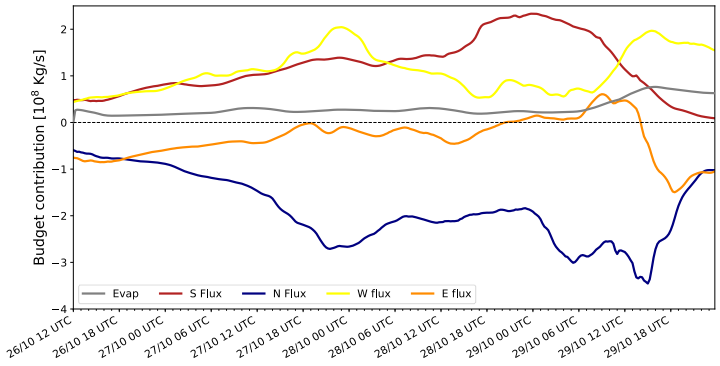

(b)

Figure 9: As in Fig. 8 but for the Vaia storm.